GlitchHiker: Uncovering Vulnerabilities of Image Signal Transmission with IEMI

Qinhong Jiang, Xiaoyu Ji, Chen Yan, Zhixin Xie, Haina Lou, and Wenyuan Xu, *Zhejiang University*

https://www.usenix.org/conference/usenixsecurity23/presentation/jiang-qinhong

This paper is included in the Proceedings of the 32nd USENIX Security Symposium.

August 9–11, 2023 • Anaheim, CA, USA

978-1-939133-37-3

Open access to the Proceedings of the 32nd USENIX Security Symposium is sponsored by USENIX.

GlitchHiker: Uncovering Vulnerabilities of Image Signal Transmission with IEMI

Qinhong Jiang
Zhejiang University

Xiaoyu Ji
Zhejiang University

Chen Yan*
Zhejiang University

Zhixin Xie
Zhejiang University

Haina Lou
Zhejiang University

Wenyuan Xu
Zhejiang University

Abstract

Cameras have evolved into one of the most critical gadgets in various applications. In this paper, we identify a new class of vulnerabilities involving the hitherto disregarded image signal transmission phase and explain the underlying principles of camera glitches for the first time. Based on the vulnerabilities, we design the `GlitchHiker` attack that can actively induce controlled glitch images of a camera at various positions, widths, and numbers using intentional electromagnetic interference (IEMI). We successfully launch the `GlitchHiker` attack on 8 off-the-shelf camera systems in 5 categories in their original packages at a distance of up to 30 cm. Experiments with 2 case studies involving 4 object detectors and 2 face detectors show that injecting one ribboning suffices to hide, create or alter objects and persons with a maximum success rate of 98.5% and 80.4%, respectively. Then, we discuss real-world attack scenarios and perform preliminary investigations on the feasibility of targeted attacks. Finally, we propose hardware- and software-based countermeasures.

1 Introduction

The proliferation of cameras enables many applications that rely on images to make critical decisions, e.g., autonomous vehicles with object detection and surveillance camera systems with face detection. The security of these applications depends on the trustworthiness of the captured images, i.e., whether the images reflect reality correctly, since a distorted image may mislead the detector. In this paper, we uncover and investigate a new class of vulnerabilities that can be exploited to *falsify* the captured images using IEMI. The falsified images can potentially cause computer vision (CV) applications to make incorrect decisions, as illustrated in Fig. 1.

Different from existing attacks against cameras [11, 16, 19, 27, 34, 37, 49, 50] that exploited image sensors as the attack surface, our work calls for attention to the "*Image Signal Transmission*" phase in a camera system, which involves transmitting the raw image signals generated by the image sensor to an image processor via a standard camera interface bus. The transmitted image signals will go through an image processing pipeline before becoming the final images or videos. Vulnerabilities of the image signal transmission have long been overlooked due to the seeming absence of an attack surface—external access to the image signals is disabled by camera design. Our work is motivated by the *bizarre camera glitches*, a phenomenon found in rare but benign scenarios on various types of cameras, including Raspberry Pi [20, 44], webcams [15, 30], and smartphones [1, 4]. As shown in Fig. 2, most of the camera glitches appeared as horizontal purple stripes overlapped across the entire image, significantly distorting the image content. Since no optical interference was present when camera glitches happened, electromagnetic interference (EMI) from the environment or other parts of the device is suspected to be one of the main culprits [7]. If true, we wonder if an attacker could falsify a camera's output images by intentionally inducing similar glitches via IEMI. However, it is unclear whether such an attack is feasible or poses a genuine threat though this phenomenon has been known for almost a decade.

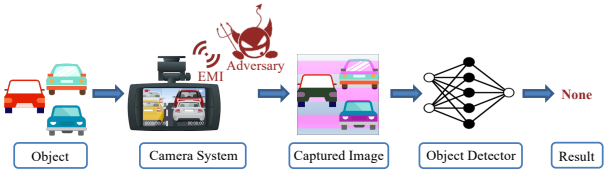

Figure 1: `GlitchHiker` attacks falsify the output images of an autonomous vehicle's camera by injecting EMI signals, which can hide the cars to be detected, resulting in collisions.

After studying a camera system's workflow, we believe the camera interface bus used for image signal transmission is a significant target for EMI coupling. Our preliminary experiment demonstrates that a strong EMI can inject interference signals into the image transmission line despite the protocol's anti-interference designs, causing random glitches similar to Fig. 2. To investigate the reason, we discover that the raw im-

* Chen Yan is the corresponding author.

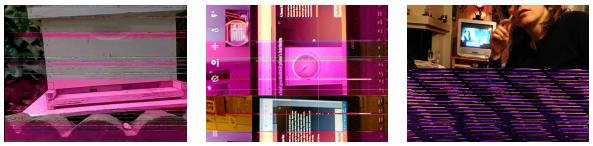

(a) Raspberry Pi [20] (b) Google Pixel [1] (c) Apple iPhone 5 [4]

Figure 2: Benign camera glitches in public reports.

age signals are designed to be transmitted by individual lines of the image sensor and are decoded according to the fixed color filter arrangement. Due to the alternating arrangement of color filters in consecutive lines, if a line missing in the transmission, e.g., caused by EMI, is not handled properly by the image processor, it can disrupt the color interpretation of the following lines during the image processing, thereby causing colorful ribbonings. In addition, we observe that if a large number of lines are missing in transmission, it will cause visible content stitching between consecutive frames.

Based on the discovered vulnerabilities of image signal transmission, we design `GlitchHiker` attack (`GH` attack in short) that can falsify a camera's output images with IEMI. Without wiring into the camera directly, `GH` attack can intentionally create camera glitches and manipulate glitch patterns' position, width and number. We successfully launch the `GH` attack on 8 off-the-shelf camera systems in 5 categories in their original packages at a distance of up to 30 cm. Proof-of-concept experiments conducted on these cameras with 2 case studies involving 4 object detectors and 2 face detectors demonstrate that injecting one ribboning can effectively reduce the reliability and performance of object detection and face detection with a maximum success rate of 98.5% and 80.4%, respectively. We discuss real-world attack scenarios, build a miniaturized attack prototype for less than $40, and investigate the attack's feasibility in a real-world scenario. Although our paper mainly studies untargeted attacks, we have performed additional preliminary investigations on targeted attacks that can hide, create and alter specific objects.

Understanding `GH` attack and analyzing the characteristics of camera glitches can help enhance future camera systems and expand the assumption on forms of image interference to prepare CV systems against a broader range of attack vectors. In summary, our contributions include:

- We discover a new class of camera vulnerabilities involving the previously overlooked image signal transmission phase in a camera system. We are the first to study and explain the camera glitch phenomenon.
- We design the `GH` attack, which can intentionally falsify a camera's output images by adding controlled glitch patterns via IEMI injection. We validate the attack on 8 off-the-shelf cameras in 5 categories with 2 case studies involving 4 object detectors and 2 face detectors.
- We discuss real-world attack scenarios and perform preliminary investigations on the feasibility of targeted attacks that can hide, create or alter specific objects.
- We suggest hardware- and software-based countermeasures.

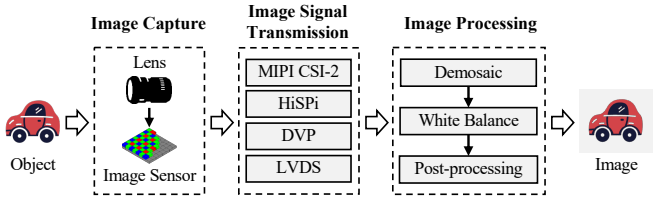

Figure 3: A simplified camera system's workflow, including image capture, image signal transmission, and image processing. Image capture and processing are typically implemented on separate hardware that transmits and receives image signals via standard camera interfaces, such as the MIPI CSI-2.

2 Camera System Preliminaries

In this section, we introduce camera systems and their known vulnerabilities. A camera system's workflow includes three typical procedures: image capture, image signal transmission, and image processing. As shown in Fig. 3, an image sensor converts ambient light to digital signals of a pixel array, which are transmitted via a standard camera interface to an image signal processor (ISP) that produces the final image or video.

2.1 Image Capture

There are two main types of image sensors, the charge-coupled device (CCD) and the complementary metal-oxide-semiconductor (CMOS). CMOS sensors currently dominate consumer products due to their low cost and power consumption. As shown in Fig. 4(a), an image sensor consists of three parts: (1) an array of photodiodes that measures the light intensity and converts it to an electrical signal, (2) a color filter array (CFA) that only allows the light of specific wavelengths to reach the photodiodes, and (3) a microlens that increases the optical fill factor. This design enables the image sensor to measure different colors at various pixels. The Bayer filter mosaic [47], also known as BGGR, RGBG, GRBG, or RGGB, is the most popular pattern for color filter arrays. Inspired by the human visual system, a typical Bayer filter mosaic is arranged with red (R), green (G), and blue (B) color filters alternatively, with the number of green filters doubling others because human eyes are more sensitive to green light.

2.2 Image Signal Transmission

Several serial and parallel buses (a.k.a. the camera interface or CAMIF) have been proposed for public and proprietary use to connect an image sensor and an image processor. For example, the Digital Video Port (DVP), Low-voltage Differential Signaling (LVDS) [46], MIPI Camera Serial Interface 2 (MIPI CSI-2) [28], and High-speed Serial Pixel Interface (HiSPi) [2]. With the rising demand for higher throughput and compatibility between hardware and software from different vendors, *MIPI CSI-2* has become the *de-facto* standard for

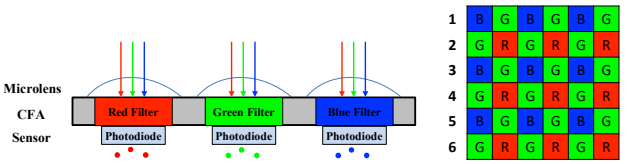

(a) Structure of a digital image sensor (b) Bayer filter mosaic

Figure 4: A typical structure of a digital image sensor and an example of color filter array.

camera interfaces and has achieved widespread adoption for its ease of use, design of anti-interference, and ability to support a broad range of camera applications. It employs MIPI D-PHY for the physical layer and high-speed differential interfaces with up to four data lanes and a shared differential clock lane to transmit image data by rows. MIPI CSI-2 defines two kinds of data packet formats in the low-level protocol: long packet used for image data transmission and short packet for interrupting frame start (FS) and frame end (FE).

2.3 Image Processing

After receiving the raw image signals, the ISP or host processor performs image processing to recover viewable images that match human perception. Despite the manufacturer algorithm differences, a standard image processing pipeline typically includes demosaic, white balance, and post-processing.

Demosaic is a process of reconstructing a full-resolution color image from the sampled Bayer-encoded image signals. The sampled Bayer-encoded image is not viewable because each pixel only measures one color, and interpolation is required to estimate the full color of each pixel in the RGB color space using information from nearby pixels [35]. Standard algorithms include direct interpolation, nearest-neighbor interpolation, and bilinear interpolation.

White balance or color balance is a color correction mechanism that compensates for the unrealistic color biases caused by CFA and light sources. White balance can be achieved in various ways, and the gray world algorithm (GWA) [23] is utilized on most cameras.

Depending on the camera application, the ISP may perform further post-processing, such as noise reduction and image compression, to provide photos or videos in the required format and quality.

2.4 Known Camera System Vulnerabilities

Existing vulnerabilities of camera systems mostly reside on the sensors in the image capture phase, e.g., the saturation [34, 49], the fundamental architecture [18], and rolling shutter mechanism [19, 37, 50] of image sensors, the reflection of lenses [27], and acoustic susceptibility of the image sensor's anti-shake head [16]. The vulnerability of image signal transmission has been rarely discovered and exploited yet. Oyama et al. [32, 33] proposed a fault injection attack on image transmission lines with the assumption of physically connecting to the MIPI CSI-2 lines. However, external access to the image sensor is disabled by the camera's design in the real world. Our work parallels with [32, 33], and we can stealthily falsify a camera's output image using IEMI without physically wiring into the image transmission lines.

3 Threat Model

3.1 Attacker's Goal and Attack Scenarios

The attacker aims to reduce the reliability and performance of camera-based computer vision (CV) systems by stealthily falsifying a camera's output images with IEMI. In particular, there may be two attack scenarios: (1) *Mislead the object detection of autonomous driving.* The attacker may fool autonomous vehicles by intentionally creating glitch patterns to hide existing objects or create fake objects in the image. Either case may cause erroneous vehicle behaviors and potentially lead to accidents. (2) *Evade the face detection of a video surveillance system.* Similarly, the attacker may avoid being detected if the captured image is falsified with IEMI.

We envision that the intentionally created glitch patterns may significantly disrupt or spoof CV systems, and we classify the attacks into three categories based on their outcomes: (1) **Hiding Attack (HA):** where an object/face in an original image disappears under the attack. (2) **Creating Attack (CA):** where a new object/face appears under the attack. (3) **Altering Attack (AA):** where an object/face in an original image is misdetected to another object/face under the attack. It is important to note that our attack is to hide, create or alter any objects/faces, i.e., untargeted attacks.

3.2 Attacker's Capabilities

We make the following assumptions for the attacker to achieve the aforementioned attacks:

Attack with EMI. Considering the attacker's goal and all possible options to trigger the camera glitches, we assume the attacker can only falsify the camera's output image by intentionally generating EMI. That is, she cannot take apart or wire into the camera, physically change objects in the camera's field of view, emit visible light and sound, or digitally hijack the camera's image transmission to the CV system, e.g., using malware.

Knowledge of the Target Camera. The attacker knows the target camera's model, and she may obtain a similar camera for assessment beforehand. For example, she may learn the design of the camera's frame rate from public documents or by reverse engineering. However, during the attack, the target camera remains as a black box, and there is no regular access to the camera's output images or inner signals.

Proximity Access to the Target Camera. We assume the attacker can physically get close to the target camera and

(a) (b) (c)

Figure 5: The camera glitches appear under the electrostatic gun (a-b) and the signal generator (c). It shows that an attacker can intentionally generate camera glitches using IEMI.

quickly place an attack device on/near the camera to prepare for the attack. This can happen when vehicles and surveillance cameras are temporarily unattended. We envision two types of potential real-world attack scenarios: contact attacks and contactless proximity attacks. Nonetheless, the attacker does not have the time to dismantle the camera and tamper with its hardware or software settings.

4 Feasibility and Vulnerability Investigation

In this section, we first investigate the feasibility of intentionally generating camera glitches and the reasons for glitch patterns. Then, we illustrate how the investigation facilitates us in identifying vulnerabilities of image signal transmission. Our investigations and experiments are conducted based on a standalone OmniVision OV5647 camera module attached to a Raspberry Pi 3B+ board through the standard MIPI CSI-2 camera interface.

4.1 Generating Camera Glitches with IEMI

Several online discussions suspected EMI as the cause of camera glitches in certain circumstances [4, 20]. These observations motivate us to investigate the feasibility of generating glitch patterns using IEMI. As a preliminary experiment, we utilize an electrostatic gun to generate high-intensity electric charge pulses at the image transmission line between the OmniVision OV5647 camera module and the Raspberry Pi 3B+ board. We report the results in Figs. 5(a) and 5(b). Also, we successfully inject similar glitch patterns in Fig. 5(c) by employing a signal generator, a power amplifier, and a magnetic probe to generating a 30 MHz sine wave. The glitch images we generated are similar to the benign cases in Fig. 2, showing purple horizontal ribboning and serious content stitching. However, these glitch patterns appeared sporadically and traversed the image.

4.2 What Goes Wrong with the Camera Systems?

After verifying the feasibility of generating camera glitches with IEMI, we are inspired to investigate the cause of glitches and what goes wrong with image signal transmission.

Investigate the Cause of Camera Glitches. Data buses are well-known to be susceptible to EMI disruption, which

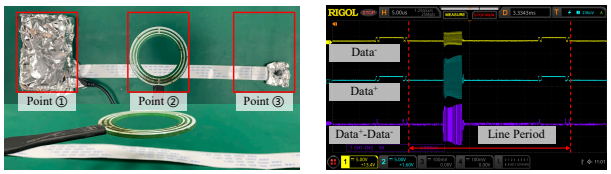

(a) Three injection points (b) Signal under strong EMI

Figure 6: (a) Illustration of the three injection points. (b) Signals of transmitting a single image line probed on the CSI lines when injecting at point ②.

couples an electric potential into the wires and affects the voltages of the transmitted signals. We use a 30 cm sunny connector and conduct an experiment to demonstrate the cause of camera glitches by moving the magnetic probe to the three injection points indicated in Fig. 6(a). The other two injection points are shielded when the probe is in one of the three points. The result shows that the glitch patterns can be induced only when the probe is placed over the transmission line at the injection point ②, implying that the glitch is caused by interfering with the image signal transmission. After confirming that the image transmission phase is disrupted, we address the following two questions.

What Goes Wrong with the Transmission Lines? MIPI CSI-2 is designed with preparation for environmental interference, and the MIPI D-PHY [29] physical layer carries differential signals on several pairs of `DATA+` and `DATA-` lines. This design is capable of rejecting common-mode interference in most cases. We wonder what goes wrong. During the injection, we monitor the `DATA+` and `DATA-` lines of the image transmission with an oscilloscope. Fig. 6(b) shows the signals measured on the `DATA+` and `DATA-`, as well as the calculated differential signal when a single line of the image is transmitted under EMI. Both data channels are affected by different levels of EMI interference, and there is still interference in the differential signal. In other words, IEMI introduces differential-mode interference into the transmission lines, causing some image signal transmission errors. In addition, we use the commands "vcgencmd set_logging level=0xc00" and "sudo vcdbg log msg" to capture the firmware log of Raspberry Pi's SoC during the injection. The result shows that there are numerous error messages in the log when the glitches appeared, indicating that various transmission errors occured.

How Does the Transmission Protocol Respond to the Errors? We carefully review the source code (`bcm2835-unicam.c` and `bcm2835-unicam.h`) of the Raspberry Pi's CSI driver and find a status register `Unicam_STA` defined to report transmission errors. Raspberry Pi implements the Checksum and ECC checking in hardware block, and errors are indicated via the `Unicam_STA` register. The Pi SoC discards the lines that encounter transmission errors[1], and sets a status bit in the `Unicam_STA` register. This does not

[1] This is confirmed by the Raspberry Pi engineers who write this driver.

increment the write pointer, so the next line received without multiple bit errors will be written to that point in the image buffer. We experimentally confirm this by analyzing the size of the captured raw data file. We use the command line "libcamera-raw -t 1000 –segment 2 -o test%03d.raw" to capture the raw frames with the resolution of 640*480 for 2 seconds. We receive a .raw file with a size of 384,000 bytes under normal circumstances. However, the size of a .raw file we receive during the attack is less than 384,000 bytes (for example, 380,928 bytes), indicating that several lines are missing.

4.3 Why Glitches Appear in Specific Patterns?

After knowing what goes wrong with the image signal transmission under EMI interference, the following question is why a few discarded horizontal lines can significantly alter the color and content of the other parts of the image. We first study the standard image processing pipeline on Raspberry Pi, and then we investigate the causes of image color and content changes, respectively.

4.3.1 The Normal Image Processing Pipeline

Raspberry Pi has two independent hardware blocks to handle the received image data packet: Unicam (CSI receiver) and ISP. The processing pipeline can be briefly summarized as follows. A buffer in Pi SoC's SDRAM is allocated for the captured image, and the start/end address of the buffer and the line pitch are passed to the Unicam. Unicam waits for the FS interrupt to write all subsequent data into this buffer. When the FE interrupt is received, the buffer is signaled as "complete" and passed to the ISP. Then, the ISP process the defined image buffer (demosaic, white balance, etc.) with whatever data is there and output the final image. However, the missing lines disrupt this pipeline, changing the captured image's color and content.

4.3.2 Investigating the Color Change

As shown in Fig. 4(b), the blue-green (B/G) and green-red (G/R) filters in the Bayer filter array are arranged in a line-alternating fashion. Half of the lines contain blue-green colors, and the other half contains green-red colors. The missing of one line may desynchronize the Bayer pattern and significantly affect the color cognition of subsequent lines. We illustrate this effect with two cases in Fig. 7.

Case 1: An image data packet is discarded. When line 2 in Fig. 4(b) is discarded, the demosaic algorithm does not know that a line is missing and works as usual. Thus, the Bayer order below line 2 swaps and becomes Fig. 7(a). The red and blue filters in Bayer are decoded as green filters, and the green filters are decoded as red or blue filters. Due to the architecture of the RGGB CFA, green values are usually higher than

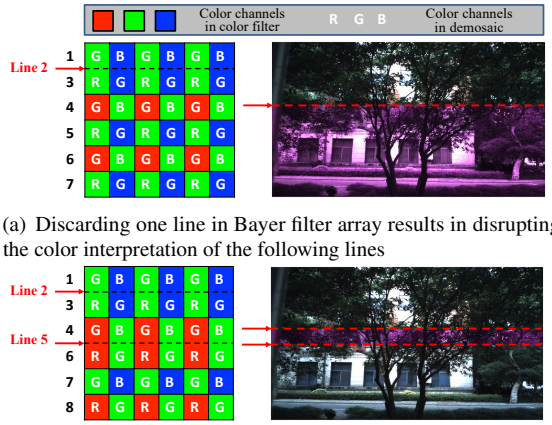

(a) Discarding one line in Bayer filter array results in disrupting the color interpretation of the following lines

(b) Discarding two lines in Bayer filter array results in the purple stripes overlapping on the image

Figure 7: Two examples illustrate why intra-frame colorful ribbonings appear. Discarding a line in (a) leads all subsequent green filters to be decoded as red and blue, and all red/blue filters to be decoded as green. In (b), removing another line can end the color discrepancy.

red and blue under normal circumstances. Therefore, after color swapping, the values of blue and red increase and the green values decrease in most cases, making the image to be purple or magenta after the process of demosaicing and white balance. In addition, discarding an odd number of lines can achieve the same outcome, but discarding an even number of lines cannot.

Case 2: Another image data packet is dropped after Case 1. As illustrated in Fig. 7(b), a second line (line 5) is discarded in the same manner, the Bayer order is swapped again, and the subsequent lines are returned to their previous state, resulting in a color stripe overlapping on the original image. In this paper, the phenomenon associated with Case 1&2 is referred to as intra-frame colorful ribboning.

Insight 1: Discarding $(2n-1)$ lines ($n \in \mathbb{N}^*$) continuously can swap the Bayer order and disrupt the color interpretation of subsequent lines and discarding $(2n-1)$ lines again ends this form of color discrepancy.

Depending on the RGB values of the source image, numerous colorful ribbonings may be induced. Fig. 8 depicts the transition of the color space resulting from the missing lines on a ColorChecker Classic. The discarding of lines converts an image's color space from a standard color space to a purple-green color space. For example, the green region in Fig. 8(a) converts into purple in Fig. 8(b), while the red region becomes green. Moreover, after color space shifting, the fourth row of six grayscale colors, including white ($(255,255,255)$) and black ($(0,0,0)$), remains unchanged. This is because the RGB values of grayscale colors are identical in all three channels and this form of swapping has no effect on them.

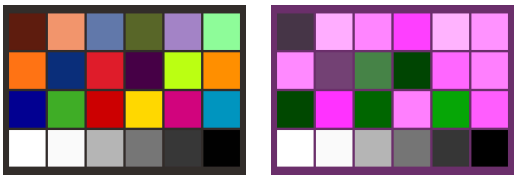

(a) Standard color space (b) Purple-green color space

Figure 8: The missing lines shift the color space of ColorChecker Classic.

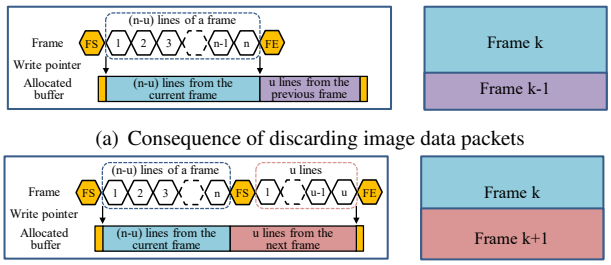

(a) Consequence of discarding image data packets

(b) Consequence of discarding both image data packets and FE/FS packets

Figure 9: Illustrations of why inter-frame content stitching appears. (a) The image is stitched with the previous frame when the FE package comes early; (b) The image is stitched with the next frame when the FE package is lost.

4.3.3 Investigating the Content Change

The discarding of lines results in a short frame; however, it is unclear why the glitch images are always complete, i.e., without being cropped. The write pointer will be advanced based on the programmed line pitch *if and only if* the line data packet contains no uncorrectable errors. The controller does not increment the write pointer after receiving a corrupted line. Therefore, it will be overwritten by the following line when the line is invalid (e.g., encounter multiple errors). Two cases may happen when several image data packets and FS/FE packets are discarded.

Case 3: Only image data packets are discarded, and a FS packet can be successfully paired with a FE packet. Assuming u image data packets are discarded in a frame, the buffer is signaled as "complete" when the FE interrupt is received though the buffer is not fully overwritten, as illustrated in Fig. 9(a). Image buffers are not memset before writing to, so a short frame will result in the last u lines of the buffer will hold the image data from a previous complete frame, resulting in content stitching between consecutive images.

Case 4: Both image data packets and FS/FE packets are discarded, and a FS packet cannot be successfully paired with a FE packet. In such a circumstance, the image buffer writing process will be severely impacted, and there are two potential conditions. (1) A FS is followed by another FS, and the write pointer loses track of the FE in this frame. The controller waits for a FE from the next frame to signal the captured frame as "complete". (2) A FE is followed by another FE, and the data of this frame may not be written into the buffer. Fig. 9(b) shows that the data of the next frame are written into the buffer until a FE packet from the next frame comes. In this paper, we refer to the two vertical desynchronization phenomenons associated with Case 3&4 as inter-frame content stitching.

Insight 2: Discarding u image data packets of a frame can cause the image to be stitched with u lines from the previous frame, and discarding u image data packets together with a FE packet can cause the image to be stitched with u lines from the next frame.

Summary. We can summarize from the above two insights that discarding lines may result in intra-frame colorful ribboning and inter-frame content stitching, but the intra-frame colorful ribboning will not appear if an even number of lines are continuously discarded. The appearance of the intra-frame colorful ribboning incidentally produces the inter-frame content stitching. However, the inter-frame content stitching is not noticeable when only a few lines are discarded. The more lines are discarded, the more prominent the inter-frame content stitching and the more distorted the captured image. Therefore, to modify the content of the captured image as little as possible, we mainly focus on the intra-frame colorful ribboning and design the injection signal to falsify glitch patterns at various positions, widths, and numbers of ribbonings.

5 Attack Design

In this section, we present `GlitchHiker`, the first attack that can intentionally induce controlled camera glitches via IEMI. The attacker's goal is to inject disruption to falsify a camera's output images to glitch patterns at a variety of positions, widths, and numbers. The attack workflow is summarized in Fig. 10. We first endeavor to find the appropriate injection frequency with the proper transmitting antenna to perform efficient glitch injection. Second, we synchronize the injection with the image signal transmission and design the controlled injection signal to manipulate the position, width, and number of glitch patterns.

5.1 Efficient Glitch Injection

Though We have verified the possibility of generating camera glitches with an electrostatic gun in Section 4.1, these glitch patterns only appeared occasionally. The effectiveness of the glitch injection is dependent on the strength of the coupled signal in the victim camera system. To increase the efficiency of glitch injection, we first consider the generation and transmission of the EM signal.

EM Signal Generation. The coupling efficiency between a victim circuit and an EM signal is determined by the frequency and amplitude of the EM signal. *(1) Signal frequency* f. We can increase the strength of the coupled signal by determining the frequency at which the victim circuit is most susceptible. Since it is difficult to examine the victim circuit's resonant frequency, we conduct a frequency sweeping test to determine the effective frequency range. *(2) Signal amplitude*

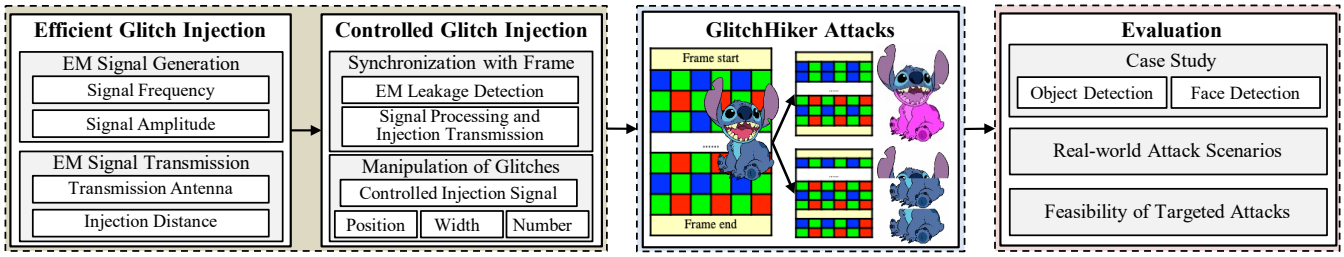

Figure 10: The attack workflow of `GlitchHiker`, including two basic building blocks: efficient glitch injection and controlled glitch injection. `GlitchHiker` attack can induce intra-frame colorful ribbonings and inter-frame content stitching images, misleading CV systems such as object detection and face detection.

Figure 11: Illustrations of efficient glitch injection, where the glitch patterns are still randomly distributed.

A. The signal generator can produce a sine wave signal with a maximum amplitude of 19 dBm (80 mW). And we implement the power amplifier in Fig. 16 to amplify the signal sufficient to undertake an IEMI attack across long distances. We investigate the relationship between the signal power and the attack distance in Fig. 18(b).

EM Signal Transmission. EM signals can be transmitted through space by the transmission antenna in electromagnetic waves. An antenna with wide-band operational capabilities would be advantageous for sweeping the frequency of the injection signal across a broad range to determine the frequency at which an efficient IEMI attack occurs. We use the magnetic field probe in Fig. 16 to perform glitch injection on a Raspberry Pi 3B+ and Fig. 11 illustrates the efficiency glitch injections at 100 MHz and -5 dBm.

5.2 Controlled Glitch Injection

After improving the injection efficiency, the following task is to make the random glitches controlled. The attacker can accomplish this by (1) synchronizing the injection with image signal transmission and (2) designing the controlled injection signal to manipulate the position, width, and number of the glitch patterns.

5.2.1 Synchronization with Image Signal Transmission

As shown in Fig. 12, we synchronize the injection with image signal transmission by EM leakage detection, signal processing, and injection signal transmission.

EM Leakage Detection. The voltage of the victim camera's data lines changes from "high" to "low" or reverses during image signal transmission, creating a sudden current in the line. This sudden current creates a magnetic field that an attacker can use to eavesdrop the timing of the image signal

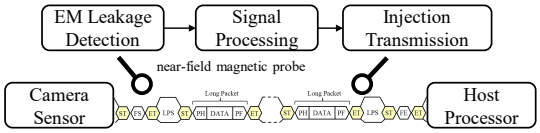

Figure 12: Illustration of synchronization mechanism. The attacker uses a near-field magnetic probe to detect the EM leakage for synchronization.

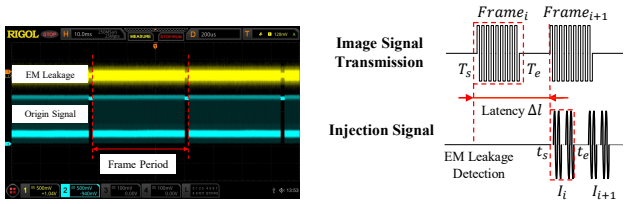

(a) EM leakage for synchronization (b) Synchronization strategy

Figure 13: (a) The relationship between the EM leakage and the original signal. We can find that the frame's start and period can be detected and measured from the EM leakage. (b) The strategy of synchronizing the injection with the image signal transmission.

transmission for synchronization. We utilize an oscilloscope, a magnetic probe, and a low noise amplifier to monitor the EM leakage and Fig. 13(a) illustrates the relationship between the EM leakage and the original signal. The result indicates that synchronizing injection timing with the image signal transmission is feasible.

Signal Processing and Injection Transmission. Our strategy of synchronization with image signal transmission is depicted in Fig. 13(b). After detecting the frame start interrupt of $Frame_i$, the arbitrary signal generator is triggered to output the injection signal into $Frame_{i+1}$ after a latency of Δl. The signal generator's latency is less than 100 ns, which is substantially shorter than the period of line transmission and can be considered constant. Furthermore, we can calculate the frame period according to the camera's frame rate to estimate the arrival of $Frame_{i+1}$ and adjust the timing of the injection signal. Thus, we can execute steady injections across continuous video frames.

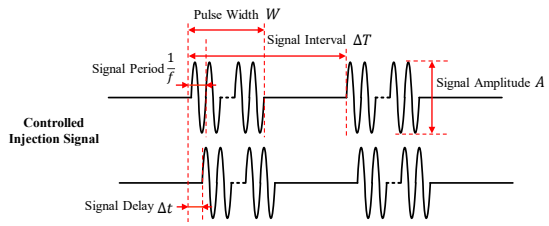

Figure 14: Illustration of the controlled injection signal. There are five configurable parameters to manipulate the position, width, and number of glitch patterns.

5.2.2 Manipulation of Glitch Patterns

We design the controlled injection signal to manipulate s frame's position, width, and number of ribbonings. Fig. 14 shows the schematic diagram of the signal we designed.

Controlled Injection Signal Designing. The controlled injection signal has five configurable parameters: signal frequency f, signal amplitude A, pulse width W, signal delay Δt, and signal interval ΔT. A controlled injection signal contains W width of the pulse signal, and ΔT denotes the time interval between two consecutive injection signals. f, A, and Δt represent the sine wave's frequency, amplitude, and delay time, respectively. We can perform various glitch injections by varying the values of these five parameters: (1) We should choose the adequate combination of f and A determined in Section 5.1 to realize the efficient glitch injection. (2) We can change Δt to do synchronization and manipulate the position of the ribboning. (3) When W is increased, more lines are discarded, resulting in more severe visible inter-frame stitching. We set W to be 100 us based on empirical value to achieve a high injection success rate while avoiding visible stitching. In addition, we evaluate the effect of the value of W on stitching in Appendix F. (4) We can change the value of ΔT to adjust the intervals between adjacent ribbonings and inject ribbonings across frames according to the camera's frame rate. ΔT can be a constant or a variable, and we show examples of ribbonings with equal and unequal intervals in Appendix B. The condition of ribbonings with unequal intervals is complex, and we set ΔT to be a constant to inject ribbonings with equal intervals to demonstrate the ability of `GH` attack.

Manipulation of the Position, Width, and Number of Purple Ribbonings. (1) *Position.* After synchronization with image signal transmission, the start position of the ribboning can be represented as $\frac{\Delta t}{1/F}$, where F is the frame rate of the camera system. We can adjust the signal delay value Δt to change the position of the glitch patterns. Fig. 15(a) shows that the ribboning gradually move downward (from left to right) with the increase of the value of Δt. (2) *Width.* Given the start position of the glitch pattern, we can manipulate a ribboning's width by adjusting the value of signal interval ΔT according to Insight 2. Fig. 15(b) shows that the ribboning gets wider with the increase of the signal interval ΔT. (3)

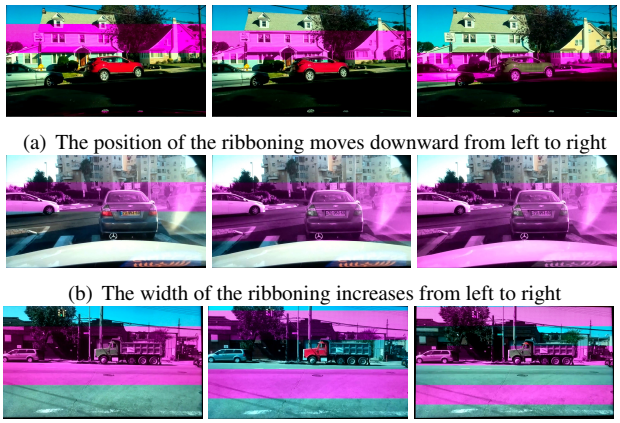

(a) The position of the ribboning moves downward from left to right

(b) The width of the ribboning increases from left to right

(c) The number of ribbonings increases from left to right

Figure 15: Results of manipulating the glitch patterns at various positions, widths, and number of colorful ribbonings.

Number. We can adjust the settings of signal delay Δt and signal interval ΔT to adjust the value of N to manipulate the number of purple ribbonings. If $\Delta t = 0$, we can set $\Delta T = \frac{1}{2*N} \cdot \frac{1}{F}$ to inject N ribbonings, and the smaller the ΔT, the denser the color stripes. Fig. 15(c) shows examples of 1, 2, 3 purple ribbonings overlapping on the image with different ΔT settings of 16.66 ms, 6.66 ms, and 4.76 ms when the frame rate is 30 fps. More examples can be found in Appendix B.

6 Evaluation

We perform `GH` attack on 8 camera systems to validate the effectiveness of the attack. Then, we evaluate the untargeted attacks on these cameras with 2 case studies involving 4 object detectors and 2 face detectors. Next, we evaluate the attack's performance regarding the ribboning number and attack distance. Finally, we discuss real-world scenarios, build a miniaturized attack prototype, and briefly investigate the attack's feasibility in a real-world scenario.

6.1 Experiment Setup

The experimental setup is shown in Fig. 16. The attack devices used in a laboratory setting include a Keysight N5712b vector signal generator for EMI signal generation, a Mini-Circuits ZHL-100W-GAN+ power amplifier or a Mini-Circuits ZHL-50W-63+ power amplifier for EMI signal amplifying, a convenient magnetic field probe (with a radius of 45mm and operating frequencies ranging from 9 kHz to 3 GHz) for EMI signal generation transmission. A RIGOL MSO8104 digital oscilloscope, a near-field probe, and a low noise amplifier (LNA) are used to monitor the EM leakage to synchronize with image signal transmission. Thus, if not otherwise specified, we maintain the experiment setup like this.

Figure 16: Illustrations of the experimental setup for investigating the performance of GlitchHiker attack.

6.2 Attack on Eight Camera Systems

We evaluate our GH attack on eight off-the-shelf camera systems in five categories, including five physically sealed consumer camera systems and three latest IoT Kits with MIPI cameras. The camera systems we tested are shown in Fig. 23, and their specs and attack results are reported in Table 1. Attaching the attack antenna to the camera shell in preparation, we run a frequency sweeping test on these cameras from 20 MHz to 1 GHz with a 10 MHz step and -5 dBm amplitude. We attach the attack antenna next to the camera's shell in advance and conduct a frequency sweeping test on these cameras from 20 MHz to 1 GHz with a step of 10 MHz at an amplitude of -5 dBm. The results show that all eight cameras are subject to our GH attack whether the camera system is physically sealed. We can induce both intra-frame colorful ribboning and inter-frame content stitching glitch patterns. During the frequency sweep test, we can achieve successful attacks at multiple frequencies, and the minimum effective injection frequency varies among camera systems due to their different circuits. Under the guidance of Section 5.2.2, we can manipulate the glitch patterns at different position, width and number by modifying the value of Δt and ΔT according to each camera's frame rate. For example, to induce one ribboning into a Blackview Dacshcam and a Xiaomi Dafang IP camera, we should set the value of signal interval ΔT to be 16.6 ms and 12.5 ms, respectively.

6.3 Case Studies

We conduct the GlitchHiker attack as a proof of concept to demonstrate the vulnerability's security impact. We place the victim camera systems in front of a monitor displaying images from a public dataset.

Attack Strategy. The attacker's goal is to reduce the reliability of camera-based computer vision systems. Unlike the works on generating adversarial examples, we do not focus on targeted adversarial attacks, which require obtaining the real-time camera images for optimization and synchronizing to precisely controlled injection, and are too overwhelming to fit our threat model. During the attack, we use the same set of signal frequency, signal amplitude, and pulse width (1 GHz, -5 dBm, and 100 us) and customize the value of signal interval ΔT based on each camera's frame rate. To increase the variety of injected glitch patterns, for each experiment, our attack strategy is to inject a ribboning with various positions inside the images and widths to cover more cases.

Evaluation Metric. We classify the fine-grained attack outcomes into three categories described in Section 3 based on the intersection over union (IoU). The details of IoU can be found in Appendix D. We use attack success rate (SR) as the evaluation metric, which is the ratio between the number of successful attacks (at least one object/face is hidden, created, or altered in the detector's output) over the total number of conducted attacks.

6.3.1 Case Study I: Object Detection

We display the 100 images selected from the BDD100K dataset [52] and send the images captured by 3 cameras (Raspberry Pi 3B+, 360 M320 Dashcam, and Blackview Dashcam) to 4 academic object detectors, including 3 one-stage object detectors (YOLO v3/v4/v5 [3, 5, 36]) and a two-stage object detector (Faster R-CNN [6]).

The attack's overall SRs are reported in Table 2, and we summarize the results regarding CV systems, attack outcomes, and camera systems. 1) *CV systems:* our attack achieves an average attack SR of 82.7%, 85.7%, 93.4%, and 98.5% against YOLO v3/v4/v5 and Faster R-CNN, where Faster R-CNN is the most fragile of the four models. 2) *Attack outcomes:* our attack achieves an average attack SR of 77.2%, 60.0%, and 27.8% for HA, CA, and AA. We can see that it is easier to achieve HA and CA than AA for these detectors, which may be because AA needs to make more fine-grained changes to the image. 3) *Camera systems:* the attack's average SRs against Raspberry Pi 3B+, 360 M320 Dashcam, and Blackview Dashcam are 90.0%, 89.7%, and 90.6%. The performance of these three camera systems appears to be very similar, although the Blackview Dashcam is slightly more vulnerable. HA may mislead autonomous vehicles to unintended operations. For example, the attacker can hide all the objects in the original image in Fig. 17(a), resulting in severe consequences such as hitting the car. CA may create a non-existent object that can lead to malicious driving behaviors. As shown in Fig. 17(b), the attacker can create a person, resulting in emergency brakes or detours. AA may cause severe traffic accidents as HA and CA do; for example, the cars in the original image may be altered to a train in Fig. 17(c).

6.3.2 Case Study II: Face Detection

We evaluate the attacks on Facenet [38] and RetinaFace [10] using ASUS Tinker Board 2, Xiaomi Dafang IP Camera, and Google Pixel One. The 100 images are selected from the WIDER dataset [51] and real-world surveillance videos. Two attack outcomes are detected: fewer people (HA) or more people (CA). Altering attack (AA) is not available.

Table 1: Feasibility of GlitchHiker attack on 8 camera systems.

Camera Systems	Manuf. & Model	Sensor (Type)	Max Res.	FPS	Physically Sealed	Attack Parameters†		Manipulation of Intra-frame Ribboning			Inter-frame Stitching‡	Attack Scenarios
						Eff. Freq. (MHz)	Max Dist. (mm)	Pos.	Wid.	Num.		
IoT Kit	Raspberry Pi 3B+	CMOS (OmniVision OV5647)	2592 * 1944	30 fps	✗	20 – 110 330 – 500 740 – 1000	82	✓	✓	✓	✓	Object Detection
	Arduino MKR Vidor 4000	CMOS (Sony IMX219 NoIR)	3280 * 2464	30 fps	✗	30 – 100 310 – 480 740 – 1000	80	✓	✓	✓	✓	Object Detection
	ASUS Tinker Board 2	CMOS (Sony IMX219)	3280 * 2464	20 fps	✗	30 – 90 310 – 480 720 – 1000	78	✓	✓	✓	✓	Face Detection
Dashboard Camera	360 M320 Dashcam	CMOS (N/A)	2560 * 1440	25 fps	✓	520 – 630 900 – 1000	40	✓	✓	✓	✓	Object Detection
	Blackview Dashcam	CMOS (N/A)	2340 * 1296	30 fps	✓	520 – 620 710 – 1000	75	✓	✓	✓	✓	Object Detection
IP Camera	Xiaomi Dafang IP Camera	1/2.7 Inch CMOS (N/A)	1920 * 1080	15 fps	✓	100 – 500 740 – 1000	32	✓	✓	✓	✓	Face Detection
Intelligent Access Control System	Baidu Dumu CM-mini	1/2.7 Inch Starlight CMOS (N/A)	1920 * 1080	25 fps	✓	630 – 1000	15	✓	✓	✓	✓	Face Detection
Smart Phone	Google Pixel One	CMOS (Sony IMX1378 Exmor RS)	3840 * 2160	30 fps	✓	30 – 100 740 – 1000	18	✓	✓	✓	✓	Face Detection

† The efficient frequency and the max attack distance are measured in our laboratory environment.
‡ These camera systems are evaluated in two case studies: object detection and face detection.

Table 2: The attack results in object detection.

Sys.	Attack Result	Target Camera System			Avg.
		Raspberry Pi 3B+	360 M320 Dashcam	Blackview Dasecam	
YOLO v3	SR*	84.3%	81.0%	82.9%	82.7%
	HA	72.8%	65.6%	69.8%	69.4%
	CA	37.0%	37.1%	50.1%	41.4%
	AA	14.9%	11.1%	23.5%	16.5%
YOLO v4	SR*	82.6%	86.8%	87.7%	85.7%
	HA	68.8%	72.2%	67.2%	69.4%
	CA	41.8%	48.8%	62.0%	50.9%
	AA	21.2%	25.1%	23.8%	23.4%
YOLO v5	SR*	94.2%	93.5%	92.5%	93.4%
	HA	79.9%	71.7%	84.0%	78.5%
	CA	67.3%	65.3%	69.6%	67.4%
	AA	24.9%	29.4%	32.3%	28.9%
Faster R-CNN	SR*	98.8%	97.3%	99.3%	98.5%
	HA	93.9%	89.2%	91.4%	91.5%
	CA	69.5%	80.1%	91.7%	80.4%
	AA	32.3%	45.3%	49.7%	42.4%

* More than one attack outcomes may appear simultaneously in a single image, resulting in SR $\neq$ HA + CA + AA.

Table 3: The attack results in face detection.

Sys.	Attack Result	Target Camera System			Avg.
		Asus Tinker	Xiaomi Dafang	Google Pixel	
Facenet	SR*	79.3%	83.6%	78.3%	80.4%
	HA	60.7%	69.8%	63.5%	64.7%
	CA	18.6%	13.8%	14.8%	15.7%
RetinaFace	SR*	69.8%	84.0%	75.2%	76.3%
	HA	56.5%	67.2%	62.5%	62.1%
	CA	13.3%	16.8%	12.7%	14.3%

* The number of faces either increases or decreases, so SR = HA + CA.

We report the attack's overall success rates on face detection in Table 3 and summarize the results regarding CV systems, attack outcomes, and camera systems. 1) *CV systems:* our attack achieved an average attack SR of 80.4% and 76.3% against Facenet and RetinaFace, which appear to be similar. 2) *Attack outcomes:* the average attack SRs of HA and CA are 63.4% and 15.0%, indicating that it is comparatively easier to hide a person from being detected than to create a new person. 3) *Camera systems:* the attack's average SRs against ASUS Tinker Board 2, Xiaomi Dafang IP Camera, and Google Pixel One are 74.6%, 83.9%, and 76.8%. The Xiaomi Dafang IP camera is the most fragile of the three cameras. For example, 6 persons are hidden in Fig. 17(d) and a non-existing person is created in Fig. 17(e) after GH attack.

Summary. The following observations are made as a conclusion: (1) End-to-end GlitchHiker attacks can significantly disrupt object detection and face detection even if only one ribboning is injected into the captured image. (2) HA and CA are easier than AA, and AA requires a more fine-grained attack design.

6.4 Impact Quantification

We quantify the attack's capability under the impact of the ribboning number and attack distance. The experiment is carried out on a standalone OmniVision OV5647 camera model attached to a Raspberry Pi 3B+.

Impact of Ribboning Number. We vary the settings of the controlled injection signal for each image to inject a different number of ribbonings ranging from 1 to 10 at equal intervals. The result of attack SRs on face detection are shown in Fig. 18(a), and we can see that the attack SR grows with the increment of ribbonings. For example, we achieve an attack SR of 93.1% in a ribboning, while 97.3% in ten ribbonings, indicating that increasing the number of ribbonings results in more modifications to the image content and a greater likelihood of modifying the IoU in the images. There is a trade-off between the attack overhead and ribboning number.

Impact of Attack Distance. We evaluate the relationship between the power level and attack distance and calculate the injection success rate as the number of images that are successfully injected over the total number of images collected

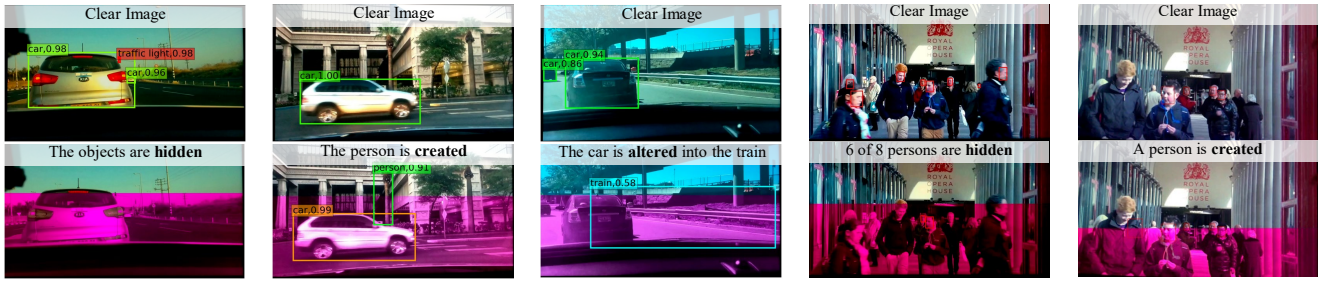

(a) (b) (c) (d) (e)

Figure 17: Illustrations of real-world attacks on object detection (a-c) and face detection (d-e).

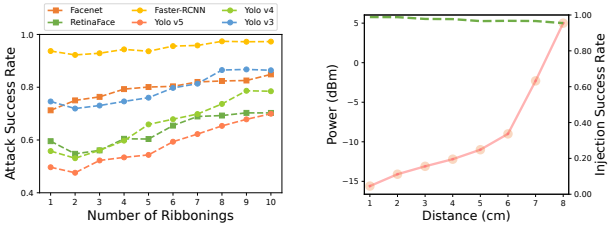

(a) Impact of ribboning number (b) Impact of attack distance

Figure 18: Performance of the attack in terms of ribboning number and attack distance.

during each attack. The results in Fig. 18(b) indicate that the long-range attack requires a more powerful signal, and the injection success rate is greater than 95% regardless of distance if it can be successfully injected. We achieve an attack distance of 8 cm in our lab experiment setting and extend the attack distance to over 30 cm by employing a PCB directional antenna (Ettus LP0410). The attacker can extend the attack distance further by selecting a magnetic resonate coupling frequency to improve the EM coupling efficiency.

6.5 Real-world Attack Scenarios

The above experiments focus on `GlitchHiker` attacks in lab environments. In the following, we discuss the challenges and plausible ways of launching this attack in real-world scenarios and demonstrate with a proof-of-concept experiment.

Potential Real-world Attack Scenarios and Challenges. We envision that there could be two types of potential real-world attack scenarios: (1) *Contact attacks:* the attacker can physically contact the target camera system and place the attack devices on/near the camera in advance to the attack opportunistically, e.g., during car wash or car maintenance; (2) *Contactless proximity attacks:* the attacker may hide the attack devices in a backpack or handbag and launch the attack when she passes by the target camera system. Considering the need for stealthiness and practicality, the attacker may face several challenges in each attack scenario. In the first contact attack scenario, the attack devices should be small and portable enough so that the attacker can place them adjacent to the unattended camera system, after which the attacker may remotely control the device and launch the attack. The attack device can also benefit from a low cost and minimal power consumption. In the second contactless proximity attack scenario, the attack devices need to support attacking from a reasonable distance, which requires the transmitted EMI signal to be powerful and directional so that it can attack successfully and avoid interfering with other electronic devices around the camera system.

Methods to Overcome the Challenges. We discuss our efforts in overcoming the above challenges of the two attack scenarios. For contact attacks, we build a miniaturized attack prototype shown in Fig. 19(a), which is less than 15 cm long and 6 cm wide and costs less than $40. The prototype consists of an antenna and an electromagnetic pulse (EMP) generator made by a microcontroller (Seeeduino XIAO) and an EMP generation circuit. The microcontroller is responsible for controlling the EMP generator to generate pulses of width ΔW at the set interval ΔT and can be controlled remotely via Bluetooth. The EMP generation circuit consists of an N-channel MOSFET, a triode, and an amplifier. As shown in Fig. 19(a), the attacker can stick the battery-powered prototype next to the target camera when it is unattended, and launch the attack remotely via the Bluetooth connection to the prototype. For contactless proximity attacks, we have managed to boost the attack distance to more than 30 cm using a basic directional antenna. To further increase the attack distance, we can implement high-performance equipment (e.g., a high-power EM amplifier, a high-directional antenna, etc.) or inject at the resonant frequency of the victim device, which will achieve the maximum injection efficiency.

Experiment in a Real-world Scenario. To investigate the attack's feasibility in a real-world scenario, we test the contact attack on a dashboard camera mounted in a vehicle as a proof-of-concept experiment. We envision that attackers may quickly enter the target vehicle during a car wash or car maintenance and attach the attack prototype to the back of the camera, as shown in Fig. 19(b). Under this setup, we perform `GlitchHiker` attack on a Blackview dashcam and send the captured images to Faster R-CNN. The experimental results demonstrate successful end-to-end attacks that achieve all of the hiding (HA), creating (CA), and altering (AA) in this scenario. In Fig. 19(c), the cars in both images are hidden

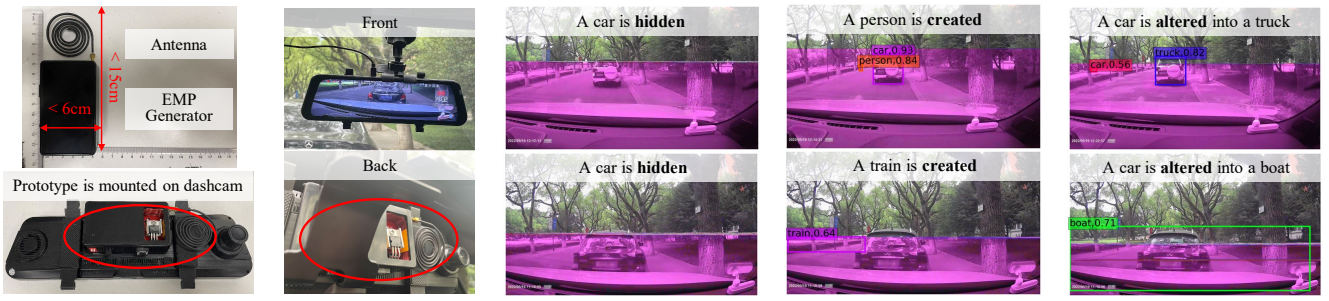

(a) Attack prototype (b) Implementation (c) HA (d) CA (e) AA

Figure 19: Illustrations of the attack prototype and the attack results on a Blackview Dashcam in a vehicle: (a) the self-built portable equipment for GH attack, (b) implementation for experimental setup, (c-e) representations of three attack outcomes.

after the attack. In Fig. 19(d), a person is created in the upper image, and a train is created in the lower image. In Fig. 19(e), a car is altered into a truck in the upper image and a boat in the lower image. We envision that the above attack outcomes may mislead an autonomous vehicle and cause severe accidents, e.g., crashing into the cars hidden in Fig. 19(c).

7 The Feasibility of Targeted Attacks

In this section, we briefly investigate the feasibility of targeted attacks that can hide, create, or alter specific objects following similar assumptions and procedures of prior works [16, 50].

Stage 1: Emulating Glitch Patterns. We develop a GH attack emulation model that takes a raw image as input and outputs an image with simulated glitch patterns. There are two steps to simulate the glitch patterns: image processing modeling and IEMI modeling. We use the high-quality linear interpolation demosaicing method proposed in [26] to transform the CMOS sensor's raw images into .jpg images and further correct the image based on the gray world algorithm (GWA) [23]. We leave the mathematical details to Appendix E. Under the guidance of Section 4.3, we can remove lines to induce intra-frame colorful ribbonings and add lines from the preceding or subsequent frame to simulate inter-frame content stitching.

Stage 2: Searching Attack Parameters. Using various combinations of injection signal parameters, we can simulate glitch patterns on prerecorded images of the target object based on the glitch pattern emulation modeling. The optimization parameters include the start position S_i and width W_i of the i-th glitch pattern, the total number of glitch patterns N, and the number of discarding lines $(2n-1)$ respectively. We seek the most effective combinations of attack parameters using a Bayesian optimization method.

Stage 3: Generating EMI Injection Signals. We map the attack parameters from our simulation to adjustable injection parameters of the EMI injection signals, including: (1) *Signal Delay* Δt. The signal delay determines the start position S_i of the ribboning in the model. (2) *Signal interval* ΔT. We can change the ribboning's width W_i by modifying the value

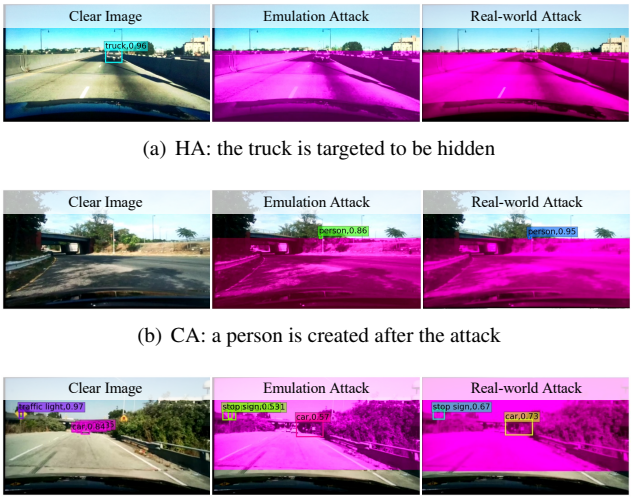

(a) HA: the truck is targeted to be hidden

(b) CA: a person is created after the attack

(c) AA: the traffic light is altered to a stop sign

Figure 20: Representative examples of the targeted attacks.

of signal Interval ΔT, and the maximum number of glitch patterns N can be expressed as $N = \lceil \frac{T_e - T_s - \Delta t}{2 \times \Delta T} \rceil$, where T_s and T_e are the start and end time of a frame. (3) *Pulse Width* W. We can increase the pulse width to discard more lines, and the relationship between the pulse width and the number of discarding lines is discussed in Appendix F.

Experiment of Targeted Attacks. Fig. 20 presents a comparison between the original, simulated attack and the real GlitchHiker attack images. Each group of images shows similar glitch patterns visually and has the same detection results from Fast-RCNN. For example, the truck in Fig. 20(a) is targeted to be hidden. A non-existing person is detected in Fig. 20(b) mistakenly. The traffic light in Fig. 20(c) is incorrectly detected as a stop sign. The results suggest that targeted attacks are feasible in an ideal experimental setup.

Practical Challenges of Targeted Attacks. Though the simulated images may look similar to those created in real attacks, there is sometimes a color difference between the real attack image and the simulated image, which is caused by the dynamically changing camera parameters such as ISO

and exposure time. We found that the detector is sensitive to such color differences and may lead to unexpected attack results. In addition, the attacker will face several significant challenges for targeted attacks in practice: (1) obtaining the camera system's output images, (2) real-time generation of adversarial examples according to the output images, and (3) synchronizing with the camera's image signal transmission for precise control of the injected glitch patterns. We leave the exploration of targeted attacks to future work.

8 Discussion

Explore the Inter-frame Content Stitching. Due to space limits, we mainly focus on the intra-frame colorful ribboning and do not discuss the inter-frame content stitching in detail. We conduct additional experiments to investigate the relationship between the pulse width and the inter-frame content stitching patterns. We also explore the attacks exploiting inter-frame content stitching in Appendix F.

Countermeasures. To alleviate the vulnerabilities, we propose hardware- and software-based countermeasures. (1) The image transmission lines should have an electromagnetic shield structure, which is the first and most effective step in preventing a malicious signal from coupling to the image transmission lines. Unfortunately, the electromagnetic shielding in these off-the-shelf camera systems is not as effective as anticipated. (2) We suggest that the camera system manufacturers utilizing the MIPI CSI-2 protocol should strictly follow MIPI Alliance Camera Working Groups' recommended approach for handling error conditions. We believe developing error handling mechanisms can deal with packet loss and prevent `GH` attacks. (3) The CV models can be protected from `GH` attacks by detecting these glitch patterns. We propose and evaluate an attack detection method by calculating the color difference between images in Appendix G.

Limitations and Future Work. The frequency step of the frequency sweeping test is so large that it is difficult to determine the resonant frequency at which injection efficiency is at its highest. We can use fine-grained frequency steps in the effective frequency range to identify the resonant frequency to improve attack performance. Furthermore, a more effective targeted attack requires further investigations and improvements. We designate these issues as our future work.

9 Related work

In the following, we summarize the existing attacks utilizing EMI and real-world adversarial attacks on CV systems.

EMI Attacks. EMI is known to jeopardize the integrity and reliability of analog sensor outputs, communication signal transmissions, and actuator behaviors. (1) *Analog sensor's outputs.* Several existing IEMI attacks target at sensors, such as microphones [21, 48], implantable cardiac devices [21], magnetic speed sensors [42], smartphones [17, 48], light sensors [39], temperature sensors [43], CCD sensors [18] and touchscreens [40, 45]. (2) *Communication signal transmissions.* Selvaraj et al. [39] presented the IEMI attack that an attacker may induce bit flips in serial communications, and Ogura et al. [31] falsified a CAN frame by EM transient pulse injection to the CAN bus. (3) *Actuator behaviors.* Dayanikli et al. [8, 9] demonstrated modulated IEMI attacks to compromise the power switches and the servo motors. Our `GH` attack focuses on the image signal transmission phase and can actively induce controlled glitch images of a camera.

Real-world Adversarial Attacks on Computer Vision Systems. Existing real-world attacks can be categorized primarily as those that interfere with the camera sensor's operation and purposely designed perturbations on the object in a special shape or color. Works in [11, 34, 49] demonstrated that strong lights or lasers could blind a camera or cause a rolling color effect, and works in [13, 16, 19, 24, 27, 37, 50, 53] showed the ability to bypass and misleading attacks against CV systems by illuminating the camera or object with modified infrared, LED, laser beams and acoustic signals. Oyama et al. [32, 33] proposed a fault injection attack by physically wiring into the camera's MIPI lines. Works in [12, 14, 22, 25] demonstrated the existence of physical adversarial examples by printing hostile perturbations as a "adversarial patch". Previous research has primarily focused on the object or the image capturing phase, whereas our `GH` attack emphasizes the security of image signal transmission. Our work highlights this new vulnerability, sheds light on its fundamental causes, demonstrates its severity impact and offers countermeasures.

10 Conclusion

In this paper, we uncover a new class of vulnerabilities in image signal transmission phase and explain the underlying principles of camera glitches for the first time. We design `GlitchHiker`, a unique attack that can actively falsify a camera's output images through IEMI. We demonstrate how the attack can disrupt off-the-shelf camera systems and deceive CV systems, discuss real-world attack scenarios and investigate the feasibility of targeted attacks. We propose both hardware- and software-based countermeasures to alleviate the vulnerability's threat.

Acknowledgments

We appreciate the anonymous reviewers' valuable comments and the Raspberry Pi engineers' patient responses. This work is supported by China NSFC Grant 62222114, 62201503, 61925109, and 62071428.

References

[1] Aaron Brown. Google pixel owners are noticing this bizarre camera glitch. https://www.express.co.uk/life-style/science-technology/739148/Google-Pixel-Camera-Purple-Lines, 2016. [Online; accessed 19-August-2021].

[2] Aptina. High-speed serial pixel (hispi) interface protocol. https://files.niemo.de/aptina_pdfs/High-Speed_Serial_Pixel_%28HiSPi%29_Interface_Specification.pdf, 2011. [Online; accessed 17-August-2021].

[3] Alexey Bochkovskiy, Chien-Yao Wang, and Hong-Yuan Mark Liao. Yolov4: Optimal speed and accuracy of object detection. *arXiv preprint arXiv:2004.10934*, 2020.

[4] bonka. Iphone 5 camera error – pink stripes. https://bareform.no/snacks/iphone5-pink-stripes/, 2012. [Online; accessed 19-August-2021].

[5] Mikel Broström. Real-time multi-object tracker using yolov5 and deep sort. https://github.com/mikel-brostrom/Yolov5_DeepSort_Pytorch, 2020.

[6] Xinlei Chen and Abhinav Gupta. An implementation of faster rcnn with study for region sampling. *arXiv preprint arXiv:1702.02138*, 2017.

[7] Daisy Palmatier. What causes interference on security cameras? https://homesecuritystore.com/what-causes-interference-on-security-cameras, 2021. [Online; accessed 19-August-2021].

[8] Gökçen Yilmaz Dayanikli. *Electromagnetic Interference Attacks on Cyber-Physical Systems: Theory, Demonstration, and Defense*. PhD thesis, Virginia Tech, 2021.

[9] Gökçen Yilmaz Dayanikli, Rees R Hatch, Ryan M Gerdes, Hongjie Wang, and Regan Zane. Electromagnetic sensor and actuator attacks on power converters for electric vehicles. In *Proceedings of 2020 IEEE Security and Privacy Workshops (SPW)*, 2020.

[10] Jiankang Deng, Jia Guo, Yuxiang Zhou, Jinke Yu, Irene Kotsia, and Stefanos Zafeiriou. Retinaface: Single-stage dense face localisation in the wild. *arXiv preprint arXiv:1905.00641*, 2019.

[11] Sharath Yadav DH and Asadullah Ansari. Autonomous vehicles camera blinding attack detection using sequence modelling and predictive analytics. Technical report, SAE Technical Paper, 2020.

[12] Ranjie Duan, Xingjun Ma, Yisen Wang, James Bailey, A Kai Qin, and Yun Yang. Adversarial camouflage: Hiding physical-world attacks with natural styles. In *Proceedings of the IEEE/CVF conference on computer vision and pattern recognition*, 2020.

[13] Ranjie Duan, Xiaofeng Mao, A Kai Qin, Yuefeng Chen, Shaokai Ye, Yuan He, and Yun Yang. Adversarial laser beam: Effective physical-world attack to dnns in a blink. In *Proceedings of the IEEE/CVF Conference on Computer Vision and Pattern Recognition*, 2021.

[14] Kevin Eykholt, Ivan Evtimov, Earlence Fernandes, Bo Li, Amir Rahmati, Chaowei Xiao, Atul Prakash, Tadayoshi Kohno, and Dawn Song. Robust physical-world attacks on deep learning visual classification. In *Proceedings of the IEEE conference on computer vision and pattern recognition*, 2018.

[15] hemmigumm. Weird red lines across webcam. https://www.dell.com/community/XPS/Weird-red-lines-across-webcam/td-p/6184452, 2018. [Online; accessed 19-August-2021].

[16] Xiaoyu Ji, Yushi Cheng, Yuepeng Zhang, Kai Wang, Chen Yan, Wenyuan Xu, and Kevin Fu. Poltergeist: Acoustic adversarial machine learning against cameras and computer vision. In *Proceedings of 2021 IEEE Symposium on Security and Privacy (SP)*, 2021.

[17] Chaouki Kasmi and Jose Lopes Esteves. Iemi threats for information security: Remote command injection on modern smartphones. *IEEE Transactions on Electromagnetic Compatibility*, 57(6):1752–1755, 2015.

[18] Sebastian Kohler, Richard Baker, and Ivan Martinovic. Signal injection attacks against CCD image sensors. In *Proceedings of the 2022 ACM ASIA Conference on Computer and Communications Security*, 2022.

[19] Sebastian Köhler, Giulio Lovisotto, Simon Birnbach, Richard Baker, and Ivan Martinovic. They see me rollin': Inherent vulnerability of the rolling shutter in cmos image sensors. In *Proceedings of Annual Computer Security Applications Conference*, 2021.

[20] ktemby. Purple artifacts in pi camera module raspivid. https://www.raspberrypi.org/forums/viewtopic.php?t=131161, 2016. [Online; accessed 19-August-2021].

[21] Denis Foo Kune, John Backes, Shane S Clark, Daniel Kramer, Matthew Reynolds, Kevin Fu, Yongdae Kim, and Wenyuan Xu. Ghost talk: Mitigating emi signal injection attacks against analog sensors. In *Proceedings of 2013 IEEE Symposium on Security and Privacy*, 2013.

[22] Alexey Kurakin, Ian Goodfellow, Samy Bengio, et al. Adversarial examples in the physical world, 2016.

[23] Ngai M Kwok, Dalong Wang, Xiuping Jia, SY Chen, Gu Fang, and Quang P Ha. Gray world based color correction and intensity preservation for image enhancement. In *Proceedings of 2011 4th International Congress on Image and Signal Processing*. IEEE, 2011.

[24] Haoliang Li, Yufei Wang, Xiaofei Xie, Yang Liu, Shiqi Wang, Renjie Wan, Lap-Pui Chau, and Alex C Kot. Light can hack your face! black-box backdoor attack on face recognition systems. *arXiv preprint arXiv:2009.06996*, 2020.

[25] Aishan Liu, Xianglong Liu, Jiaxin Fan, Yuqing Ma, Anlan Zhang, Huiyuan Xie, and Dacheng Tao. Perceptual-sensitive gan for generating adversarial patches. In *Proceedings of the AAAI conference on artificial intelligence*, 2019.

[26] Henrique S Malvar, Li-wei He, and Ross Cutler. High-quality linear interpolation for demosaicing of bayer-patterned color images. In *Proceedings of 2004 IEEE International Conference on Acoustics, Speech, and Signal Processing*, 2004.

[27] Yanmao Man, Ming Li, and Ryan Gerdes. Ghostimage: Remote perception attacks against camera-based image classification systems. In *Proceedings of the 23rd International Symposium on Research in Attacks, Intrusions and Defenses ({RAID} 2020)*, 2020.

[28] MIPI alliance. Mipi camera serial interface 2 (mipi csi-2). https://www.mipi.org/specifications/csi-2, 2019. [Online; accessed 18-July-2021].

[29] MIPI Alliance. Mipi d-phy. https://www.mipi.org/specifications/d-phy, 2021. [Online; accessed 18-July-2021].

[30] OD42. Webcam purple lines. https://h30434.www3.hp.com/t5/Notebook-Video-Display-and-Touch/Webcam-purple-lines/td-p/7854587, 2020. [Online; accessed 19-August-2021].

[31] Hiroto Ogura, Ryunosuke Isshiki, Kengo Iokibe, Yuta Kodera, Takuya Kusaka, and Yasuyuki Nogami. Electrical falsification of can data by magnetic coupling. In *Proceedings of 2020 35th International Technical Conference on Circuits/Systems, Computers and Communications (ITC-CSCC)*, 2020.

[32] Tatsuya Oyama, Shunsuke Okura, Kota Yoshida, and Takeshi Fujino. Backdoor attack on deep neural networks triggered by fault injection attack on image sensor interface. In *Proceedings of the 5th Workshop on Attacks and Solutions in Hardware Security*, 2021.

[33] Tatsuya Oyama, Shunsuke Okura, Kota Yoshida, and Takeshi Fujino. Experimental study of fault injection attack on image sensor interface for triggering backdoored dnn models. *IEICE Transactions on Fundamentals of Electronics, Communications and Computer Sciences*, 2021.

[34] Jonathan Petit, Bas Stottelaar, Michael Feiri, and Frank Kargl. Remote attacks on automated vehicles sensors: Experiments on camera and lidar. *Black Hat Europe*, 11(2015):995, 2015.

[35] Rajeev Ramanath, Wesley E Snyder, Griff L Bilbro, and William A Sander. Demosaicking methods for bayer color arrays. *Journal of Electronic imaging*, 11(3):306–315, 2002.

[36] Joseph Redmon and Ali Farhadi. Yolov3: An incremental improvement. *arXiv preprint arXiv:1804.02767*, 2018.

[37] Athena Sayles, Ashish Hooda, Mohit Gupta, Rahul Chatterjee, and Earlence Fernandes. Invisible perturbations: Physical adversarial examples exploiting the rolling shutter effect. In *Proceedings of the IEEE/CVF Conference on Computer Vision and Pattern Recognition*, 2021.

[38] Florian Schroff, Dmitry Kalenichenko, and James Philbin. Facenet: A unified embedding for face recognition and clustering. In *Proceedings of the IEEE conference on computer vision and pattern recognition*, 2015.

[39] Jayaprakash Selvaraj, Gökçen Yılmaz Dayanıklı, Neelam Prabhu Gaunkar, David Ware, Ryan M Gerdes, and Mani Mina. Electromagnetic induction attacks against embedded systems. In *Proceedings of the 2018 on ACM Asia Conference on Computer and Communications Security*.

[40] Haoqi Shan, Boyi Zhang, Zihao Zhan, Dean Sullivan, Shuo Wang, and Yier Jin. Invisible finger: Practical electromagnetic interference attack on touchscreen-based electronic devices. In *Proceedings of 2022 IEEE Symposium on Security and Privacy (SP)*, 2022.

[41] Gaurav Sharma, Wencheng Wu, and Edul N Dalal. The ciede2000 color-difference formula: Implementation notes, supplementary test data, and mathematical observations. *Color Research & Application*, 30(1):21–30, 2005.

[42] Yasser Shoukry, Paul Martin, Paulo Tabuada, and Mani Srivastava. Non-invasive spoofing attacks for anti-lock braking systems. In *Proceedings of International Conference on Cryptographic Hardware and Embedded Systems*. Springer, 2013.

[43] Yazhou Tu, Sara Rampazzi, Bin Hao, Angel Rodriguez, Kevin Fu, and Xiali Hei. Trick or heat? attack on amplification circuits to abuse critical temperature control systems. In *Proceedings of the 2019 ACM SIGSAC Conference on Computer and Communications Security*, 2019.

[44] u/Breakr007. Noise on new pi noir camera connected to pick zero w board. what could be causing this? https://www.reddit.com/r/raspberry_pi/comments/67hpb0/noise_on_new_pi_noir_camera_connected_to_pick/, 2017. [Online; accessed 19-August-2021].

[45] Kai Wang, Mitev Richard, Chen Yan, Xiaoyu Ji, Sadeghi Ahmad-Reza, and Wenyuan Xu. GhostTouch: Targeted attacks on touchscreens without physical touch. In *Proceedings of the 31st USENIX Security Symposium (USENIX Security 22)*, 2022.

[46] Wikipedia contributors. Low-voltage differential signaling — Wikipedia, the free encyclopedia. https://en.wikipedia.org/w/index.php?title=Low-voltage_differential_signaling&oldid=1021691966, 2021. [Online; accessed 12-August-2021].

[47] Wikipedia contributors. Bayer filter — Wikipedia, the free encyclopedia. https://en.wikipedia.org/w/index.php?title=Bayer_filter&oldid=1089033345, 2022. [Online; accessed 7-June-2022].

[48] Zhifei Xu, Runbing Hua, Jack Juang, Shengxuan Xia, Jun Fan, and Chulsoon Hwang. Inaudible attack on smart speakers with intentional electromagnetic interference. *IEEE Transactions on Microwave Theory and Techniques*, 69(5):2642–2650, 2021.

[49] Chen Yan, Wenyuan Xu, and Jianhao Liu. Can you trust autonomous vehicles: Contactless attacks against sensors of self-driving vehicle. *Def Con*, 24(8):109, 2016.

[50] Chen Yan, Zhijian Xu, Zhangyuan Yin, Xiaoyu Ji, and Wenyuan Xu. Rolling colors: Adversarial laser exploits against traffic light recognition. In *Proceedings of the 31st USENIX Security Symposium (USENIX Security 22)*, 2022.

[51] Shuo Yang, Ping Luo, Chen-Change Loy, and Xiaoou Tang. Wider face: A face detection benchmark. In *Proceedings of the IEEE conference on computer vision and pattern recognition*, 2016.

[52] Fisher Yu, Haofeng Chen, Xin Wang, Wenqi Xian, Yingying Chen, Fangchen Liu, Vashisht Madhavan, and Trevor Darrell. Bdd100k: A diverse driving dataset for heterogeneous multitask learning. In *Proceedings of the IEEE/CVF conference on computer vision and pattern recognition*, 2020.

[53] Zhe Zhou, Di Tang, Xiaofeng Wang, Weili Han, Xiangyu Liu, and Kehuan Zhang. Invisible mask: Practical attacks on face recognition with infrared. *arXiv preprint arXiv:1803.04683*, 2018.

Appendix

A Responsible Disclosure

We have reported our findings, including the vulnerable devices, a thorough description of the vulnerability, and proof of concept to the MIPI Alliance and the camera system manufacturers. We presented the practical steps required to reproduce a simplified attack version. In addition, we provided our hardware- and software-based countermeasures.

B Glitch Patterns

Ribbonings with both equal and unequal intervals. When ΔT is a constant, the ribbonings are evenly spaced throughout the image in Fig. 21(a), whereas when ΔT is a variable, the stripes overlap at unequal intervals in Fig. 21(b).

(a) Injection with equal interval (b) Injection with unequal interval

Figure 21: Colorful ribbonings injected with (a) equal intervals when ΔT is a constant and (b) unequal intervals when ΔT is a variable on an OmniVision OV5647 camera.

Ribbonings at Different Number. We can modify the value of ΔT to induce different numbers of purple ribbonings overlapping on the same image. Fig. 22 shows the examples, we configure ΔT as 16.6 ms, 8.31 ms, 5.56 ms, 4.15 ms, 3.32 ms, 2.77 ms, 2.38 ms, 2,09 ms, and 1.86 ms to induce purple ribbonings range from one to nine separately. The frequency, amplitude, cycles and delay of the signal are configured as 100 MHz, 5 Vpp, 3000 and 0, respectively.

C Evaluation of GH attack.

The camera systems we evaluate are shown in Fig. 23, including 5 physically sealed consumer camera systems and 3 latest IoT Kits in their orig-inal packages. Our experiments show that EMI attacks can successfully inject glitch patterns, including intra-frame colorful ribboning and inter-frame content stitching, into all 8 off-the-shelf camera systems. Note

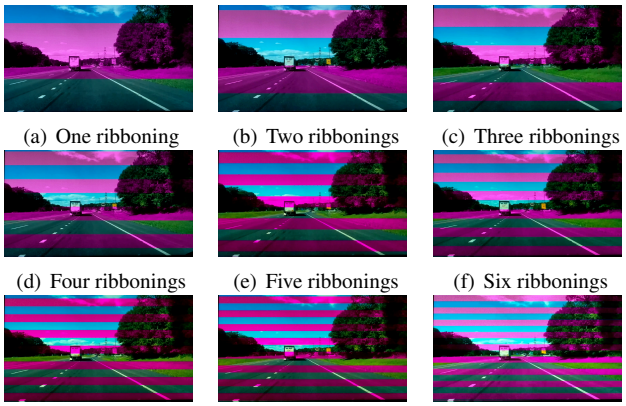

(a) One ribboning (b) Two ribbonings (c) Three ribbonings
(d) Four ribbonings (e) Five ribbonings (f) Six ribbonings
(g) Seven ribbonings (h) Eight ribbonings (i) Nine ribbonings

Figure 22: Illustrations of one to nine ribbonings that are injected into the same image.

that all camera systems except the 3 IoT Kits are physically sealed, and we do not make any modifications to these devices. We have learned their sensor type, maximum resolution, and frame rate from public documents.

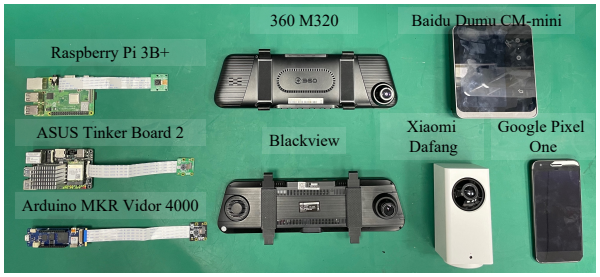

Figure 23: The 8 camera systems tested in the evaluation.

D Explanations of IoU.

IoU is commonly used to evaluate a box's prediction accuracy compared to an original or ground truth box, which is a measure of the area of overlap between two bounding boxes, as a proportion of area of overlap, area of union. If $\text{IoU}\left(b_1^{(l_1)}, b_2^{(l_2)}\right) > 0.5$, where l_i is the label of the bounding box b_i, we suppose b_1 and b_2 are at the same position. We use $b_o^{(l_o)}$ and $b_a^{(l_a)}$ to represent the box before and after GH attack. We measure fine-grained misleading attacks in three categories: (1) **Hiding Attack:** there is a bounding box $b_o^{(l_o)}$ in an original image, but the box at the same position disappears after the GH attack. (2) **Creating Attack:** there isn't a bounding box $b_o^{(l_o)}$ in an original image, but the box $b_a^{(l_a)}$ appears after the GH attack. (3) **Altering Attack:** there is a bounding box $b_o^{(l_o)}$ in an original image and a bounding box $b_a^{(l_a)}$ at the same position in a disupted image after the GH attack, where $l_a \neq l_o$.

We can summarize from the evaluation results of GH attack on face recognition as followings: (1) GH attack primarily affects face detection process when compared to face recognition, and our attack can hide a person from detection or create a fake face in the non-face area, which is then recognized as an enrolled person. (2) To improve the attack SR, the attacker should inject ribbonings into the area around a person's eyes, nose, and mouth.

E `GlitchHiker` Attack Patterns Emulation

To estimate the red value $\hat{R}(i,j)$ or blue value $\hat{B}(i,j)$ at a green pixel in the position (i,j), we can express as $\hat{X}(i,j) = \overline{X}(i,j) + \alpha\Delta_G(i,j)$. where $\overline{X}(i,j) = \frac{1}{k}\sum X(i+m, j+n)$, $X \in \{R,B\}$, $(i+m, i+n)$ is the position of neighboring red/blue pixels in a cross pattern, and k is the number of the red/blue pixels. $\Delta_G(i,j)$ is the gradient of G at that location and α is a gain parameter to control the applied correction. The gradient of the pixel at location (i,j) is $\Delta_X(i,j) \triangleq X(i,j) - \frac{1}{k}\sum X(i+m, j+n), X \in \{R,G,B\}$. After demosaicing, the red, green and blue value of a pixel in the position (i,j) will be further corrected by the white-balance diagonal matrix. So the green values of pixels in the image can be expressed as $G'(i,j) = \hat{G}(i,j)$, the red and blue values are $R'(i,j) = \hat{R}(i,j) \times (K_g/K_r)$, $B'(i,j) = \hat{B}(i,j) \times (K_g/K_b)$ respectively.

F Inter-frame Stitching

We investigate the relationship between the attack signal's pulse width W and the inter-frame content stitching pattern. As shown in Fig. 24, the inter-frame content stitching pattern becomes more prominent as the pulse width W increases (Figs. 24(a) to 24(c)). As shown in Figs. 24(b) and 24(d) to 24(f), when the pulse width W is constant, a different start position of the glitch pattern will result in different parts of the object being dropped.

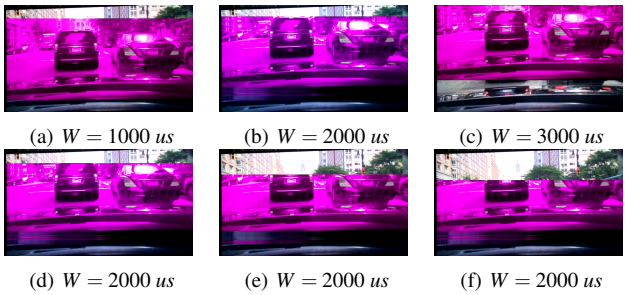

(a) $W = 1000\ us$ (b) $W = 2000\ us$ (c) $W = 3000\ us$
(d) $W = 2000\ us$ (e) $W = 2000\ us$ (f) $W = 2000\ us$

Figure 24: Illustration of inter-frame content stitching images with varied attack parameters.

We also investigated methods that use inter-frame content stitching patterns to attack the face detection system, with some representative examples shown in Fig. 25. Inter-frame content stitching patterns can cause persons in an image to both disappear (Figs. 25(a) to 25(c)) and reappear (Figs. 25(d) to 25(f)).

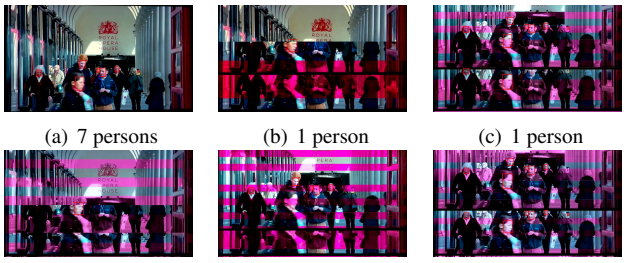

(a) 7 persons (b) 1 person (c) 1 person

(d) 2 persons (e) 9 persons (f) 12 persons

Figure 25: Illustration of a face detection attack that exploits inter-frame content stitching.

G Detecting the Images Under the Attack

We use the method in [41] to transform the image from RGB to CIE Lab color space to compute the color difference between the two images. We select six groups of images for color difference calculation, with each group containing 30 normal images and 30 images under our `GlitchHiker` attack. The results are shown in Fig. 26(a). The vertical red dash line in the center of Fig. 26(a) separates the normal images from the attacked images, and it is evident that the color difference value of the normal image in Fig. 26(b) is only affected by the environment and the camera. While the color difference value of the attacked image increases or falls dramatically and changes with the injected glitches in Fig. 26(c). For example, the average value of color difference for normal images in the fourth group is 1.12, but the maximum value under the attack might reach 3.97.

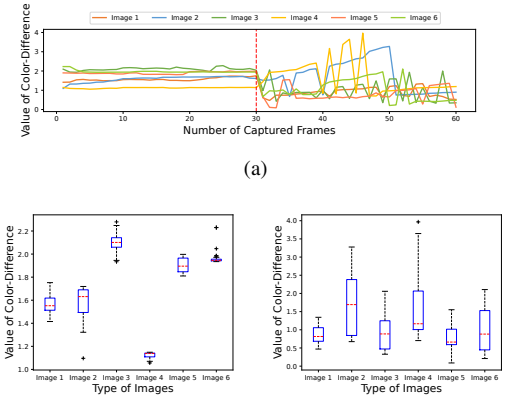

(a)

(b) (c)

Figure 26: Results of the color difference between images.